Undersampled MRI reconstruction using edge-weighted ℓ_1 norm minimization

C. Hu[1], X. Qu[2], D. Guo[2], L. Bao[1], S. Cai[1], and Z. Chen[1]

[1]Department of Physics, Xiamen University, Xiamen, Fujian, China, People's Republic of, [2]Department of Communication Engineering, Xiamen University, Xiamen, Fujian, China, People's Republic of

Introduction

MRI, a widely used analytical tool for medical diagnosis, is burdened by slow data acquisition. An effective way to speed up MRI is to undersample k-space. However, undersampling often violates the Nyquist-Shannon sampling theorem, resulting in aliasing artifacts in reconstructed MR images. Some artifacts blur edges, which usually contain significant information for pathological diagnosis, such as vascular disease and tumor border detection. To better recover the edge information, we propose an edge-weighted iterative thresholding (EWIT) algorithm for undersampled MRI reconstruction. EWIT is implemented on the base of the iterative thresholding (IT) algorithm [1,2], a fast algorithm solving the ℓ_1 norm minimization for compressed sensing (CS) MRI [3,4]. Reconstruction results indicate that EWIT yields more precise reconstructions than IT, especially for the edge recovery.

Methods

CS aims to reconstruct a $N\times 1$ signal $\mathbf{x}$ from far fewer M ($M << N$) measurements than Nyquist sampling rule by exploiting the sparsity of the signal $\mathbf{x}$ in certain transform domain, such as wavelet (WT). WT is a multiscale representation of images. Image edge features exhibit high directional oritentation and spatial correlated in the WT domain, and therefore can be located very effectively. To better recover the MR image edges, we propose the following edge-weighted model by pluging two weighting matrices into the objective function of constrained ℓ_1 norm minimization problem: $\min_{\mathbf{c}} \|(\lambda\mathbf{W}_a + (1-\lambda)\mathbf{W}_b)\times\mathbf{c}\|_1$, $s.t.\ \mathbf{y} = \mathbf{F}_u\mathbf{\Psi}\mathbf{c}$. $\mathbf{c}$ is the sparse represention of MR image vector $\mathbf{x}$ with WT transform $\mathbf{\Psi}$ ($\mathbf{x} = \mathbf{\Psi}\mathbf{c}$). $\mathbf{F}_u = \mathbf{U}\mathbf{F}$ is undersampled Fourier transform, where $\mathbf{U}$ is a $M\times N$ undersampling matrix and $\mathbf{F}$ represents the forward Fourier transform. $\mathbf{W}_a(i,i) = 1/(\mathbf{c}_s^k(i)\cdot\mathbf{c}_{s+1}^k(i))$ and $\mathbf{W}_b(i,i) = 1/I(\mathbf{c}(i))$ are two diagonal weighting matric for the correlation and orientation information of image edges in WT domain. $\mathbf{c}_s^k(i)$ is the i th entry of $\mathbf{c}$ in the k th subband at scale s, $I(\cdot)$ is the orientation information function detailed by Ref. [5]. λ ($0\le\lambda\le 1$) is a tradeoff between $\mathbf{W}_a$ and $\mathbf{W}_b$.

Results and discussion

The MR image used for simulations is T_2 weighted and obtained from a 1.5T GE MRI scanner, as shown in Fig. 1. À trous WT with spline biorthogonal filters and four decomposition levels is used as the sparsifying transform. Cartesian and radial sampling patterns are used for k-space undersampling, as shown in Fig. 2. As Cartesian sampling needs more measurements for acceptable reconstruction, the sampling rate for Cartesian sampling pattern is set to 0.3 (30% measurements) in simulation, which is 20% more than radial sampling pattern. Peak signal-to-noise ratio (PSNR) is adopted to quantify the difference between the MR images reconstructed from fully sampled and undersampled k-space. Comparison of reconstructions using IT and EWIT is given Fig. 3. The zoomed in labeled regions displayed in Fig. 3 indicate that EWIT recovers the edges with better sharpness than IT. The sharp edges are more consistent with the fully sampled MR image. As IT and EWIT optimize the ℓ_1 norm minimization, curve of PSNR versus ℓ_1 norm sparsity in Fig. 4 is employed to discuss the reconstruction accuracies of IT and EWIT with equivalent $\|\mathbf{c}\|_1$. Fig. 4 indicates that EWIT leads to a more precise reconstruction than IT with fixed ℓ_1 norm sparsity, especially for middle and high value of $\|\mathbf{c}\|_1$.

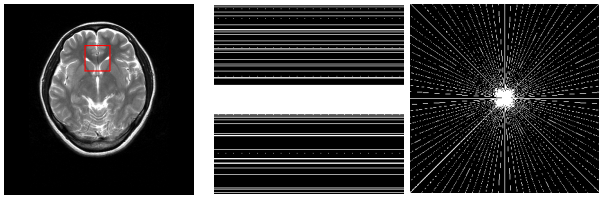

Fig. 1 T_2 weighted MR image from 1.5T GE MRI scanner.

(a) **(b)**

Fig. 2 Cartesian (a) and radial (b) sampling patterns.

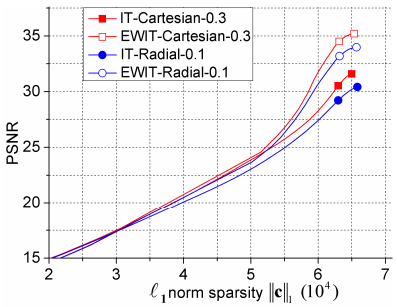

Fig. 4 PSNR versus ℓ_1 norm sparsity. The sampling rates for Cartesian and radial sampling patterns are 0.3 and 0.1, respectively.

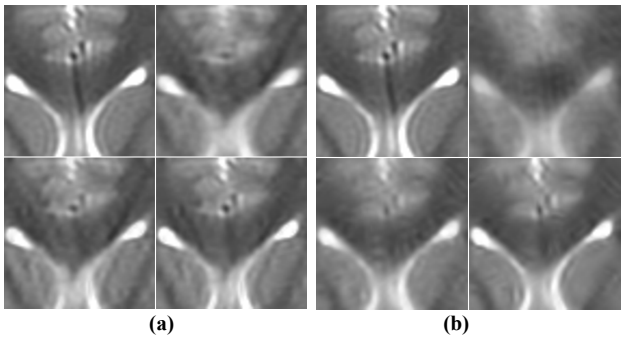

(a) **(b)**

Fig. 3 Comparison of zoomed in reconstructed regions labeled in Fig. 1. (a) and (b) are reconstructions from Cartesian and radial sampling patterns. The top left, top right, down left, and down right parts are reconstructed from fully sampled k-space, zero-filled k-space (PSNR for Cartesian and radial sampling are 27.9 dB and 21.6 dB), IT (PSNR for Cartesian and radial sampling are 31.6 dB and 30.4 dB), and EWIT (PSNR for Cartesian and radial sampling are 35.2 dB and 34.0 dB), respectively.

Acknowledgment

This work was supported by by the NNSF of China under Grant 10774125 and the Research Fund for the Doctoral Program of Higher Education of China under Grant 200803840019. Xiaobo Qu and Di Guo were supported by Postgraduates' Oversea Study Program for Building High-Level Universities from the China Scholarship Council.

References

[1] Drori I. *EURASIP J. Adv. Sig. Pr.* (2007) 195–204.
[2] Qu X, et al. *Inverse Probl. Sci. Eng.* 18 (2010) 737–758.
[3] Candès E, et al. *IEEE Trans. Inf. Theory* 52 (2006) 489–509.
[4] Donoho D. *IEEE Trans. Inf. Theory* 52 (2006) 1289–1306.
[5] Qu X, et al. *WCICA* (2008) 2437–2441.